Polymer Degradation and Stability 222 (2024) 110700

Contents lists available at ScienceDirect

Polymer Degradation and Stability

journal homepage: www.journals.elsevier.com/polymer-degradation-and-stability

Effects of UVC irradiation on polystyrene for healthcare packaging: Study by FTIR and Raman spectroscopy with thermoluminescence

C. Boronat [a,b,*], V. Correcher [b], J. García-Guinea [c], J.C. Bravo-Yagüe [d]

[a] Department of Inorganic Chemistry, Faculty of Sciences, National University of Distance Education (UNED), Av. de Esparta s/n, Madrid 28232, Spain
[b] Department of Environment, Centre for Energy, Environment and Technology Research (CIEMAT), Av. Complutense 40, Madrid 28040, Spain
[c] Department of Geology, National Museum of Natural Sciences (MNCN), The Spanish National Research Council (CSIC), St. Jose Gutierrez Abascal 2, Madrid 28006, Spain
[d] Department of Analytical Chemistry, Faculty of Sciences, National University of Distance Education (UNED), Av. de Esparta s/n, Madrid 28232, Spain

ARTICLE INFO

Keywords:
Polystyrene
Healthcare packaging
Ultraviolet C radiation
Fourier transform infrared spectroscopy
Raman spectroscopy
Thermoluminescence

ABSTRACT

The interaction between ultraviolet C radiation (UVC) and polystyrene (PS) materials has been investigated, particularly in post-packaging irradiation processes for healthcare applications. Effective UVC penetration through PS materials, regardless of their thickness (0.16 and 0.40 mm) has been observed. However, the penetration effectiveness could be affected by the thickness of the PS material. Achieving optimal post-packaging UVC treatment requires a thorough evaluation of chemical composition and material thickness, especially in pharmaceutical and medical packaging industries.

Preliminary results reveal minimal degradation in UVC-irradiated PS packaging samples, as supported by FTIR and Raman spectroscopy characterization. Minor variations could be attributed to intrinsic PS materials properties and/or their respective background, rather than the influence of UVC radiation. Consequently, PS materials exhibit resilience under the experimental conditions following UVC irradiation treatment. Furthermore, a comprehensive analysis of thermoluminescence (TL) emissions evaluates several commercial dosimeter materials for UVC radiation detection. The TLD-100 and TLD-200 dosimeters show potential as UVC detectors, displaying distinct responses linked to the non-ionizing component of UVC radiation at 310 °C and in the range of 150–250 °C, respectively. However, the TLD-400 and GR-200 dosimeters are not suitable for UVC detection due to their spread TL emissions considering intensity and curve shape.

This UVC-TL analysis consistently detects radiation in the proposed commercial dosimeter materials one-hour post-exposure, providing assurance that healthcare materials have been irradiated. Such analysis enhances reliability during extended UVC exposures, offering valuable insights for industries employing UVC-irradiated materials, particularly in healthcare applications.

1. Introduction

Disinfection and sterilization of plastic materials are essential requirements in a wide range of industries, ensuring safety and efficacy in food production, water treatment, textile manufacturing and healthcare [1–8]. In both medicine and the pharmaceutical industry, accurate disinfection and sterilization of equipment, devices, instruments and environments are fundamental to prevent hospital-acquired infections and maintain patient well-being [1,2]. It is necessary to maintain safety and compliance with quality standards, as sterility safeguards against risks such as reduced drug effectiveness and potential threats to public health from microbial contamination [8,9].

In this sense, radiation exposure is a widely employed method of sterilization commonly used in these sectors [2,9]. Such method inactivates and destroys the DNA of microorganisms using radiation sources such as non-ionizing and ionizing radiation, ensuring complete sterility even after packaging. While beta and gamma radiation are prevalent in healthcare applications [2,4,8,9], alternatives options include infrared radiation, electron-beam welding and ultraviolet radiation (UV) [1,2,5,7]. In recent years, UV radiation has gained

* Corresponding author at: Department of Inorganic Chemistry, Faculty of Sciences, National University of Distance Education (UNED), Av. de Esparta s/n, Madrid 28232, Spain.
E-mail address: cecilia.boronat@ccia.uned.es (C. Boronat).

https://doi.org/10.1016/j.polymdegradstab.2024.110700
Received 19 December 2023; Received in revised form 6 February 2024; Accepted 12 February 2024
Available online 14 February 2024

prominence as a significant technology to ensure the highest cleanliness and sterility standards in these sectors [1,5,7]. UV radiation is generally considered non-ionizing radiation and is categorized into three types based on its wavelength: UVA (320–400 nm), UVB (280–320 nm) and UVC (100–280 nm). Among them, UVC radiation is widely recognized for its exceptional germicidal efficacy, destroying the genetic material of bacteria, viruses and other microorganisms, making them unable to replicate and cause infections. The germicide action of UVC radiation is primarily attributed to its ability to damage the DNA and RNA of microorganisms, leading to their inactivation [1]. This intricate process showcases the potential of UVC radiation as a powerful tool in the fight against infectious diseases, making it an invaluable resource in pharmaceutical and medical industries, where it is employed to disinfect and sterilize various surfaces and materials [1,5,7]. These include surgical equipment, medical devices, cleanrooms and operating rooms, personal protective equipment (such us disposable and surgical face masks, respirators, coveralls and goggles), laboratory instruments, healthcare tools and pharmaceutical product packaging, among others [1,2,5,7,9].

Polystyrene (PS) is a widely known thermoplastic polymer synthesized through the polymerization of repetitive styrene units (C_8H_8), as depicted in the subsequent chemical formula (Fig. 1a). PS has become as a prevalent material in the pharmaceutical and medical sectors owing to its excellent properties and adaptability [10].

This polymer has many advantageous attributes for medical applications, including low density, transparency, dimensional stability, low cost, excellent processability and compatibility with radiation sterilization methods [10]. In the healthcare field, PS finds application in laboratory equipment, such as tissue culture and Petri dishes, in the production of containers, trays, medical device components and thermoformed products, including epidurals, catheters, and heart pump components, as well as medical packaging [10–12]. PS competes favorably with other polymers like polypropylene (PP), polyvinyl chloride (PVC) and acrylic in packaging solutions for laboratory materials, kits and trays [10]. In terms of chemical resistance, PS is not resistant to aliphatic, aromatic, cyclic ethers, chlorinated organic solvents, ketones, acids and bases. Nevertheless, it exhibits moderate resistance to higher molecular weight long-chain alcohols, bleaches, as well as dilute aqueous acids and alkalis. Notably, it demonstrates resilience against low molecular weight alcohols, ethylene oxide and various disinfectants [10]. In the context of sterilization methods, PS undergoes specific challenges due to its low heat distortion temperature, making it unsuitable for dry and moist heat sterilization (i.e., autoclaving), which could lead to undesirable warping and deformation of this polymer. However, PS exhibits remarkable stability when exposed to gamma radiation, owing to its high aromatic content, where the electron cloud within its structure effectively absorbs radiation and prevents the formation of reactive free radicals. As a result, PS materials can be exposed to multiple doses of gamma and electron-beam radiation without compromising their integrity [10]. Additionally, PS is resistant to UV radiation, further increasing its suitability for certain applications [10]. According to Andrady et al. [13], UVC radiation may cause changes in the chemical and physical properties of PS material, including: (i) chain scission and a decrease in mechanical strength resulting from a *photo-oxidation* process that breaks chemical bonds within the polymer (i.e., C–H and C–C scissions, among others) [14,15]; (ii) initiation of polymerization and/or degradation reactions due to *radical formation* (i.e., peroxy, hydroperoxide intermediates and polystyryl radicals, among others) [15]; (iii) alterations of chemical and physical characteristics by the *emergence of functional groups* within the polymer structure [15]; (iv) disintegration of pigments or colorants present in the polymer, also known as *bleaching effect* and/or *yellowing* [16]; (v) *variations in optical properties*, affecting transmittance/ absorbance or reflectance features [13]; and/or (vi) an increased risk of breakage or failure under cyclical loads due to *reduced fatigue resistance* [13,17]. Consequently, this degradation severely compromises the mechanical and tensile properties of the polymer, making it unusable over an unpredictable timeframe [18].

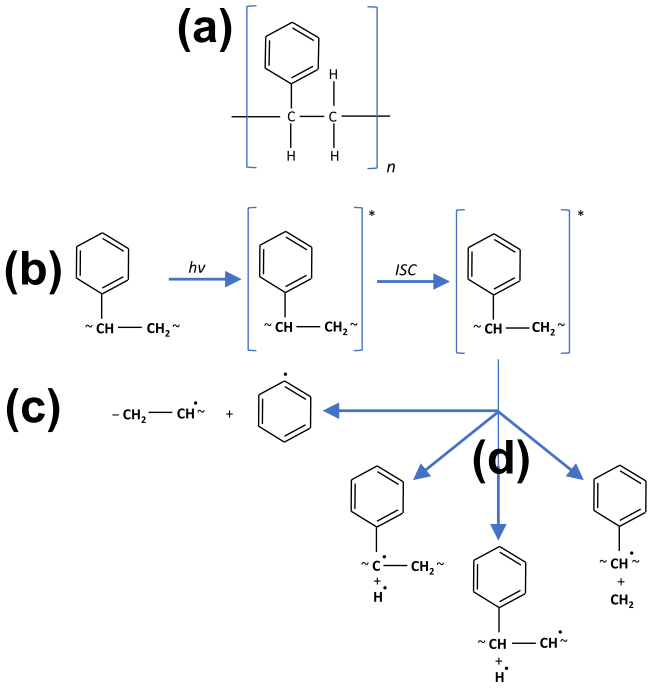

Fig. 1. (a) Molecular structure of polystyrene (C_8H_8), consisting of –CH_2– units and a mono-substituted benzene ring pendant group. The *photo-oxidative degradation* of PS occurs through radical processes, as illustrated in (b), where the formation of the triplet state takes place following light absorption by the benzene ring. Subsequently, (c) shows the dissociation of the C_6H_5–C bond, and (d) demonstrates the formation of C–H and C–C bonds (Figure adapted from Yousif and Haddad [17]). Please note that ISC stands for intersystem crossing.

The *photo-degradation* and *photo-oxidation* phenomenon of PS material have been widely studied [10,17,19–21]. *Photo-degradation* process can occur both in the absence of oxygen (resulting in chain breaking or cross-linking) and in the presence of oxygen (leading to *photo-oxidative degradation*). The process mentioned above is induced by UV radiation and other catalysts (or both), often accelerated at elevated temperatures. Furthermore, when PS material is exposed to UV radiation in the presence of air (*photo-degradation*), it can cause discoloration (*yellowing*), removal or reduction of color (*bleaching effect*), cross-linking, gradual embrittlement and chain scission due to oxidation [14–16]. In an industrial context, the *yellow discoloration* is a notable adverse effect of PS aging, particularly when exposed outdoors [17]. This process involves the formation of peroxy radical (–O–O$^{\bullet}$) and hydroperoxide intermediates (–OOH), leading to the dissociation of a polystyryl radical ($C_6H_5CH_2^{\bullet}$) and subsequent formation of carbonyl compounds (C=O) [15]. Studies have identified ketone carbonyl groups (C=O) in photo-irradiated PS through Fourier transform infrared spectroscopy (FTIR) analyses, manifested as increased absorption peaks around 1730–1745 cm^{-1} [17,19]. The study of PS *photo-degradation* process remains controversial due to the presence of impurities and irregularities within the material, including hydroperoxides (–OOH), aromatic carbonyl groups (C=O), olefin bonds (C_nH_{2n}) and chain peroxide linkages (–O–O–), which could initiate radical oxidation [15,17]. The exposure of PS to UV and visible light with wavelengths ($\lambda < 400$) nm results in the generation of radicals. The specific characteristics of these radicals depend on the spectral composition of the light and the irradiation conditions [22]. Moreover, the end groups of PS or ketonic impurities (C=O) absorb light with wavelengths up to 300 nm [22].

The absorption of light by the benzene ring initiates the excitation to singlet states, as depicted in Fig. 1b. These singlet states are subsequently transformed into the triplet state through intersystem crossing (ISC). In the next stage of the reaction involving the triplet state of

benzene, one of the following two modes occurs: (1) the triplet energy of the excited benzene may lead to the dissociation of the C_6H_5–C bond, as shown in Fig. 1c. And (2), the triplet energy excitation can be transferred through intramolecular energy transfer processes to the C–H or C–C bonds, as illustrated in Fig. 1d. During the *photolysis* of PS in the absence of oxygen, a critical step is proposed to be the scission of a C–H bond. These complex reactions underscore the intricate nature of PS *photodegradation* under diverse environmental conditions.

Furthermore, when using UV radiation as a sterilization method, it is fundamental to consider at least two essential aspects: (1) assessing the potential damage that radiation exposure may cause upon this particular polymer, and (2) detecting the presence of UVC radiation treatment in the material. For such purposes, FTIR and Raman spectroscopy and thermoluminescence (TL) are suitable techniques for determining both aspects. Despite the importance of these techniques, there has been limited research on the analysis of packaging materials exposed to UVC radiation, particularly polymeric materials such as PS [17]. Therefore, further exploration of these techniques in the context of UVC-irradiated materials holds the potential to enhance our understanding of their performance and suitability for critical applications.

Thus, both FTIR and Raman spectroscopy offer valuable insights into the structural and molecular properties of PS, a commonly used material for pharmaceutical and medical packaging [2,9,10]. FTIR could be a suitable tool for examining potential conformational changes and microscopic deformations of PS packaging materials, based on the fundamental vibrational motions of functional groups within the polymer crystal lattice. This technique provides a detailed understanding of the structural properties of materials at the molecular level without the need for chemical or physical sample pretreatment. Additionally, FTIR offers a non-invasive method to assess the integrity and composition of PS materials to ensure its suitability for critical applications [23]. On the other hand, Raman spectroscopy is equally significant, and it complements FTIR technique by providing information about the vibrational and rotational energy levels of molecules. Raman spectroscopy is a valuable tool for investigating crystallinity, stress and molecular arrangement within PS materials, shedding light on their suitability for use in healthcare packaging. This technique offers a non-destructive and highly precise method to assess the physical and chemical properties of the PS material [23].

Furthermore, while UV radiation finds application in the healthcare sectors in many countries, there is currently no established method for discriminating UV-irradiated materials, especially PS employed in medical and pharmaceutical packaging. The absence of a reliable methodology presents a challenge for regulatory authorities in their search for a tool to ensure precise labelling and/or the validation of standardized procedures for assessing the total UV dose absorbed. This tool would rely on the identification of UV-irradiated materials through alterations in their physical, chemical and biological properties [24–26]. In this context, TL emerges as one of the most efficient, suitable, cost-effective and precise methods for such purpose. TL is based on the emission of light from a dielectric solid sample, semiconductor or insulator, following exposure to ionizing or non-ionizing radiation, either of artificial or natural source. As part of the heating analysis, a photomultiplier tube captures the TL signal, which is recorded as a function of either temperature or wavelength. The resultant graph, referred to as a glow curve or TL curve, displays distinct patterns in luminescent intensity and shape, directly linked to the UV dosage and the rate of heating [27]. This technique offers substantial potential in the identification of UV exposure in materials commonly used in healthcare packaging, thereby guaranteeing adherence to established quality and safety standards.

There exist several detectors and dosimeters capable of detecting and recording UVC radiation, especially critical in the context of healthcare applications. These devices include synthetic dosimeters and electronic instruments with diverse compositions, including TLD-100 (LiF: Ti, Mg), TLD-200 (CaF_2: Mn), TLD-400 (CaF_2: Dy), and GR-200 (LiF: Mg, Cu, P), among others [26]. As a result, their compositions, genic characteristics, structures and typomorphic properties can be determined by TL technique and other methodologies, wherein several luminescent emissions could be attributed to structural, surface, intrinsic and extrinsic defects.

This study presents preliminary findings related to the effect of UVC radiation on commercial TL dosimeters (TLDs), namely TLD-100, TLD-200, TLD-400, and GR-200, placed under PS materials of different thicknesses (0.16 and 0.40 mm). The objective is to evaluate their UVC-TL responses to radiation that passes through the plastic samples. In addition to this, FTIR and Raman spectroscopy have been employed to characterize PS materials and investigate potential chemical and structural alterations induced by UVC exposure.

2. Materials and methods

This study was carried out on PS samples with different thickness of 0.16 mm (PS 1) and 0.40 mm (PS 2). The chemical and structural characterization of these plastic samples was performed using ATR-FTIR and Raman spectroscopy. Infrared absorption spectra of the samples were acquired at room temperature (RT), covering the wavenumber range from 4000 to 400 cm^{-1}. This analysis was conducted using a Spectrum FT-IR-4100 spectrometer equipped with the ATR PRO ONE Accessory (ATR-FTIR) and controlled by Spectra Manager® software, supplied by JASCO (Tokyo, Japan). The spectral resolution employed for these measurements was set to 4 cm^{-1}. Additionally, Raman spectroscopy was carried out using a Thermo Fisher DRX Raman microscope with 1 μm spatial resolution at RT, 20x objective of the confocal microscope and a laser source at 532 nm of 6 MW in mode laser power at 100 %. The Raman spectra were recorded from 3500 to 70 cm^{-1} with a spectral resolution of 1.92 cm^{-1}.

UVC exposure was conducted for 1 h at RT using an automated irradiator developed at CIEMAT [28]. This irradiator enabled UV illumination through a TUV-6W Hg lamp emitting at 254.7 nm, with a UV irradiance value of 0.03 W m^2 at a distance of 10 cm. Commercial dosimeters, specifically LiF: Ti, Mg (TLD-100), CaF_2: Dy (TLD-200) and CaF_2: Mn (TLD-400), provided by Harshaw Chemical Company (Ohio, USA), each measuring $0.32\times0.32\times0.09$ cm^3, were utilized as UVC detectors. Additionally, LiF: Mg, Cu, P (GR-200) discs with dimensions of 4.5 Ø 0.8 mm^3, supplied by Beijing Shiying Radiation Detector Works (China), were here employed. These TLDs were placed under PS samples to investigate the extent of radiation that could pass through the plastic, potentially reaching the pharmaceutical and medical materials during post-packaging irradiation.

Before the subsequent irradiation, TLDs were subjected to annealing at 400 ± 1 °C for 1 h employing an electrical oven to remove any residual information, followed by 1 h of cooling rate. The UVC radiation effect was characterized by analyzing the TL properties of the aforementioned detectors. TL measurements were conducted using an automated Risø TL reader model TL DA-12, equipped with an EMI 9635 QA photomultiplier [29]. The emission was analyzed through a FIB002-blue filter (provided by Melles-Griot Company), peaking at 320–480 nm, with a full width at half maximum (FWHM) of 80 ± 16 nm and 60 % of transmittance. Furthermore, the TL reader was equipped with a ^{90}Sr / ^{90}Y source with a dose rate of 0.011 Gy s^{-1}, calibrated using a ^{137}Cs photon source in a secondary standard laboratory [30]. All the TL measurements were carried out with a linear heating rate of 5 °C s^{-1}, starting from RT up to 400 °C, within a N_2 atmosphere. A second TL readout of the TLDs was performed to determine the background signal caused by incandescence and detector noise; this background signal was directly subtracted from the TL data.

3. Results and discussion

3.1. Sample characterization

3.1.1. Fourier transform infrared spectroscopy

The aim of this characterization is to comprehensively investigate the UVC radiation effect on PS samples with different thicknesses (0.16 and 0.40 mm). As previously outlined [10,17,19–21], exposure of PS to UVC radiation can initiate a *photo-oxidation* process characterized by three distinct steps: (i) *Initiation*, which arises from the absorption of UV radiation, causing chromophores to enter an excited state. When the absorbed energy cannot be dissipated, scission occurs (i.e., C–H and C–C); (ii) *Propagation*, where free radicals mobilize, facilitated by oxygen in the polymer matrix. These radicals abstract atoms from the polymer, striving for stabilization, unintentionally inducing further destabilization and propagating additional radicals (i.e., peroxy, hydroperoxide intermediates and polystyryl radicals); and (iii) *Termination*, marking the final stage of a free radical reaction when two free radicals combine to achieve stabilization, concluding the propagation cycle. These reactions can break bonds, fragment polymers into smaller units, or lead to cross-linkages with adjacent segments. Simultaneously, they generate new groups, which may undergo subsequent oxidation, cross-linking, or both. This process could generate various free radicals, contributing to a decrease in molecular weight [17]. Delving into the specifics of how UV radiation precisely impacts polymer chain breakdown, it is crucial to note that *photo-oxidative* degradation involves intricate molecular transformations. These include the formation of cross-linkages and the production of chemical species such as carbonyl compounds (C=O). These detailed molecular processes significantly influence the structural integrity, mechanical properties and thermal stability of the material [17]. Specifically, cross-link generation during the *photo-oxidative degradation* holds the capacity to enhance material rigidity and molecular cohesion, thereby fortifying structural integrity through the reinforcement of the polymer network. However, this enhancement may be offset by an increased susceptibility to fragility. Alterations in the molecular structure, including cross-link formation and the introduction of novel functional groups, can impact the thermal stability of PS. Such effects may manifest as changes in decomposition temperature or the ability of the material to endure extreme thermal conditions [17]. Thus, this factor could suggest a possible substantial influence on the efficacy of UVC irradiation for healthcare industry PS packaging materials, underscoring the need to assess its effects on maintaining the sterility and quality of such materials.

FTIR spectroscopy allows us to gain insights into the formation of new functional groups and chemical bonds during the *photo-oxidative degradation* of PS material, providing valuable information about the molecular changes occurring in the material. With this aim, we have analyzed FTIR spectra, from 4000 to 400 cm^{-1}, comparing non-irradiated and 1 h UVC-irradiated PS samples with different thicknesses, as depicted in Fig. 2 (a and b). To be clearer, the response has been normalized and is provided in Fig. 2 (c and d), revealing possible differences in the signal after UVC irradiation treatment. Additionally, the assignment of the observed FTIR bands is given in Table 1. For this purpose, it has been followed the standard procedure of plotting

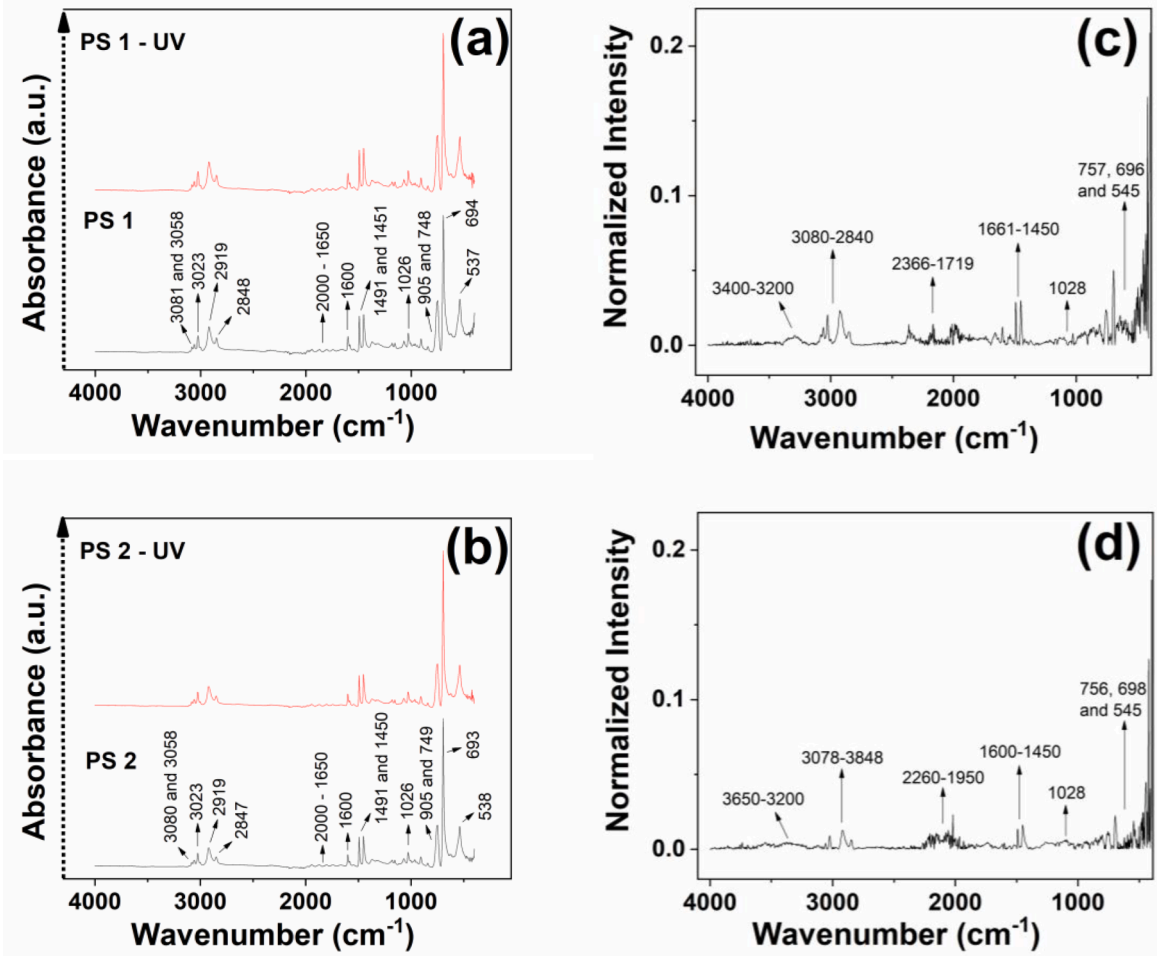

Fig. 2. FTIR and normalized FTIR spectra of non-irradiated and UVC irradiated polystyrene packaging samples with different thicknesses: (a and c) PS 1 (0.16 mm) and (b and d) PS 2 (0.40 mm). Note that the signal of the UVC-irradiated PS samples has been intentionally shifted to avoid spectral overlapping.

Table 1
Assignment of vibrational modes for observed FTIR bands in polystyrene packaging materials.

Wavenumber (cm^{-1})	Assignment of vibrational modes
3100–3000	Aromatic =C–H symmetric stretching vibrations (benzene ring, unsaturated C–H bonds)
2950–2800	CH_2 asymmetric and symmetric stretching vibrations (methylene group, saturated C–H bonds)
2000–1650	Benzene fingers
1600, 1491, 1450	Aromatic C=C stretching vibrations on the vinyl group of the benzene ring (C_6H_5–CH=CH_2)
1026	C–O stretching modes
905, 748, 693, 537	Aromatic C–H out-of-plane bending and angular deformation of the C–H group in the aromatic ring

transmission (in %) against wavenumber (in cm^{-1}), where the identified minima in the transmission spectra align with the absorption peaks associated with the molecules and functional groups.

As shown in Fig. 2 (a and b), both non-irradiated and 1 h UVC-irradiated PS samples display characteristic bands corresponding to the vibrational modes of the PS molecule, as illustrated in Fig. 1a. These characteristic FTIR peaks, distinctly outlined in Fig. 2 (a and b), are observed in the current infrared absorption spectrum and provide valuable insights into the strength of the bonds within the material, as detailed further on. The FTIR spectra indicate that, at this point, the extent of damage to different bonds in the polymer is almost negligible. However, it is essential to acknowledge that other studies have indicated that such alterations in bond strength increase with extended irradiation times [19,31].

Thus, the FTIR spectrum of the PS samples, Fig. 2 (a and b), reveals distinct absorption peaks at specific wavenumbers: (i) 3080, 3058 and 3023 cm^{-1}, which can be attributed to the symmetric stretching vibrations of the aromatic =C–H bonds in the benzene ring (unsaturated C–H); and (ii) at 2919 and 2848 cm^{-1}, corresponding to the asymmetric and symmetric stretching vibrations of the CH_2 methylene groups (saturated C–H) [32,33]. Furthermore, (iii) three notable absorption peaks at 1600, 1491 and 1451 cm^{-1} could be associated with the stretching vibrations of the aromatic C=C bonds in the vinyl group (CH_2=CH–) of the benzene ring [32,33]. Additionally, (iv) distinct absorption peaks centred at 905, 748, 694 and 537 cm^{-1} could be attributed to the out-of-plane bending of aromatic C–H bonds and angular deformation of the C–H groups within the aromatic ring [31,34]. These specific peaks, along with several emissions from 2000 to 1650 cm^{-1}, indicate the presence of a single substituent on the benzene ring [32]. Finally, an absorption peak at 1026 cm^{-1} could be associated with the presence of the C–O group [33].

Previous research have offered valuable findings into the impact of UV radiation on the FTIR spectra of PS [19,21,35,36]. These studies have revealed noticeable changes in the molecular structure of this polymer, as well as alterations in the intensities and positions of its characteristic absorption peaks. For instance, Yaseen et al. [19] investigated the impact of UV irradiation on PS films containing *Cephalexin Schiff bases*. Their FTIR spectrum revealed a substantial increase in the intensity of the C=O group absorption band after irradiation (at 1730 cm^{-1}), confirming the *photo-degradation* process of the PS material as previously explained. Notably, the absorption band corresponding to C–C bonds (at 1328 cm^{-1}) remained unaffected during irradiation. In a recent study [35], the synergistic effect of UV radiation and a chemical treatment (with nitric acid) on the biological degradation of PS was explored. Through their FTIR analysis, authors confirmed the emergence of a sharp and intense peak at 1716 cm^{-1} after UV treatment, which corresponds to aliphatic ketones and suggesting the incorporation of oxygen molecules into the PS matrix. A similar peak at 1720 cm^{-1}, previously observed by Davidson et al. [36] following UV-ozone treatment, indicated enhanced hydrophilicity due to continuous UV exposure. Furthermore, the intensity of the peak at 3741 cm^{-1} increased post-UV treatment, accompanied by the appearance of new peaks at 3608 cm^{-1} and 1647 cm^{-1}, representing O–H and C–C stretching vibrations, respectively. Additionally, in a study conducted by Sikandar Shah et al. [21], the impact of UVC irradiation was investigated at different exposure times. Their findings indicated that UV irradiation significantly reduces the molecular weight of this polymer, suggesting the degradation of PS macromolecules due to irradiation. Moreover, the study revealed that the number of chain scissions per polymer increased with prolonged irradiation, indicating an accelerated rate of PS degradation over time.

As illustrated in Fig. 2 (c and d), the normalized FTIR spectra of both non-irradiated PS samples and those irradiated with UVC for 1 h displayed minimal changes, with differences of less than 5 % (PS 1) and 2 % (PS 2) of absorbance, respect to the mean value after UVC treatment. This observation underscores the resilience of the bands in PS FTIR spectra against UVC radiation treatment, indicating their resistance to additional degradation. Nevertheless, it is essential to highlight a few subtle alterations, as detailed below:

(i) Upon analyzing the normalized FTIR spectra for PS 1 sample (0.16 mm) following UVC irradiation in Fig. 2c, we observe subtle alterations in the characteristic bands, suggesting minimal changes in its molecular structure. In the 3400–3200 cm^{-1} range, a decrease in signal intensity could suggest a reduction in hydroxyl functional groups (O–H). Diminished signals in the 3080–2840 cm^{-1} range might indicate a decrease in aliphatic C–H stretching vibrations. An increase around 2366–1719 cm^{-1} could be associated with the enhancement of the benzene fingers and due to ketone carbonyl groups (C=O), while it is almost negligible (1 %). Reduced signals in the 1661–1450 cm^{-1} range may indicate alterations in aromatic C=C stretching or C–H bending vibrations. At approximately 1028 cm^{-1}, a decline suggests modifications in C–O stretching functional groups. Moreover, an increase in the 1000–810 cm^{-1} range could indicates the presence or intensification of specific functional groups, possibly related to aromatic C–H out-of-plane bending vibrations. Decreases at 757, 696 and 545 cm^{-1} bands suggest modifications in certain molecular vibrations, possibly linked to bending of C–H bonds.

(ii) In comparison with Fig. 2d, the 3650–3200 cm^{-1} range for PS 2 sample (0.40 mm) after UVC irradiation shows an increase, suggesting enhancements in O–H stretching vibrations that could be due to a *photo-oxidation* process in the PS 2 material, even though it is almost minimal. In the 3078–2848 cm^{-1} range, an increase and a shift to lower wavenumbers for the bands centred at 3919 and 2848 cm^{-1}, could be associated with modifications in aliphatic stretching vibrations of unsaturated C–H bond of the benzene ring and saturated C–H bond of the methylene group, which could induce the disruption of C–H stretching vibrations of both aromatic and aliphatic groups in the polymeric chain. An increase around 2260–1950 cm^{-1} could be linked to the intensification of the benzene fingers. Increased signals in the 1600–1450 cm^{-1} range suggest alterations in aromatic C=C stretching vibrations on the vinyl group of the benzene ring (C_6H_5–CH=CH_2) and/or C–H bending vibrations. The 1028 cm^{-1} band remains unaffected, indicating the stability of the C–O stretching modes. Furthermore, a decrease in signal intensity in the 1260–790 cm^{-1} range indicates changes in specific functional groups, such as phenyl or methylene groups, indicating potential structural modifications within the polymeric chain. Around 756 cm^{-1}, an increase suggests modifications in certain chemical bonds (i.e., aromatic C–H out-of-plane bending vibrations). The signals at 756, 698 and 545 cm^{-1} increase, indicating alterations in specific molecular vibrations, possibly related to aromatic C–H out-of-plane bending and angular deformation of the C–H group in the aromatic ring.

In summary, these results suggest that neither of the PS packaging samples exhibits significant degradation following UVC irradiation treatment, as observed in the conducted measurements. The observed minimal differences appear to be inherent to the characteristics of the PS

materials (i.e., crystalline structure, molecular weight distribution, additives, among others) and/or may be associated with their respective histories (i.e., prior environmental exposure, manufacturing processes, storage conditions, among others), rather than the UVC irradiation.

In the case of PS 1 sample (0.16 mm thickness), the minimal variation in signal intensity within the 3400–3200 cm^{-1} range suggests that the hydroxyl functional groups (O–H) and aliphatic C–H stretching vibrations remain largely unaffected. Similarly, the nearly negligible changes in the region corresponding to benzene ring groups and carbonyl functionalities (C=O) do not seem to be indicative of substantial degradation. Conversely, regarding PS 2 sample (0.40 mm thickness), the slight differences observed in the O–H stretching vibrations within the 3650–3200 cm^{-1} range do not significantly point to a pronounced *photo-oxidation* process within the PS 2 material. The minor shifts and increases in intensity for bands centred at 3919 and 2848 cm^{-1} within the 3078–2848 cm^{-1} range are not indicative of substantial modifications in aliphatic stretching vibrations. Besides, the minimal changes in the 1600–1450 cm^{-1} range do not strongly suggest significant alterations in aromatic C=C stretching vibrations or C–H bending vibrations. Understanding the complex interaction between PS thickness and its response to UVC radiation is crucial for ensuring the effectiveness of UVC treatment post-packaging, especially in the context of healthcare applications, where guaranteeing product sterility and quality is imperative.

3.1.2. *Raman spectroscopy*

In addition to the FTIR analysis, we have used Raman spectroscopy for the characterization of the PS samples. This technique serves as a complementary approach to offer a more comprehensive and thorough understanding of potential chemical and structural changes in PS materials. To archive this aim, we have compared Raman spectra (from 3500 to 70 cm^{-1}) of both non-irradiated and 1 h UVC-irradiated PS samples with different thicknesses, as illustrated in Fig. 3 (a and b). To enhance clarity, the response has been normalized and is presented in Fig. 3 (c and d), revealing potential variations in the signal following UVC irradiation treatment. Furthermore, Table 2 provides the assignment of the observed Raman bands. Our methodology adhered to the standard procedure of plotting Raman intensity (in cps) against Raman shift (in cm^{-1}), with the identified features in the Raman spectra corresponding to the vibrational modes of the molecules and functional groups. As appreciated in Fig. 3 (a and b), non-irradiated PS samples exhibit characteristic bands corresponding to the vibrational modes of the PS [23,37–39].

Notable bands are located at: (i) 3049 cm^{-1}, which correspond to =C–H stretching vibrations of the aromatic ring [23]. And two bands at higher Raman shift peaked at 2900 cm^{-1} and 2842 cm^{-1} due to C–H stretching vibrations of the aliphatic group and CH_3 stretching vibrations, respectively [23]; (ii) 1601 cm^{-1}, linked to C=C stretching vibrations of the aromatic ring [23,37,38]; (iii) 1450 cm^{-1}, associated with aromatic ring stretching and CH_2 scissoring vibrations [23]; (iv) a group of three bands peaked at 1198, 1181 and 1154 cm^{-1}, corresponding to C–C stretches [37] and aromatic C–H in-plane bending vibrations [23]; (v) 1030 cm^{-1}, related to C–H in-plane deformation [38]; (vi) 1000 cm^{-1} (the most intense band in both PS samples) associated with C=C–H deformation [23], and ring breathing mode [37,38]; (vii) 796 cm^{-1}, linked to aromatic rings vibrations due to *gauche-gauche* conformation of the aliphatic chain [39] and C–H out-of-plane deformation [23,38]; (viii) 620 cm^{-1}, which corresponds to ring out-of-plane

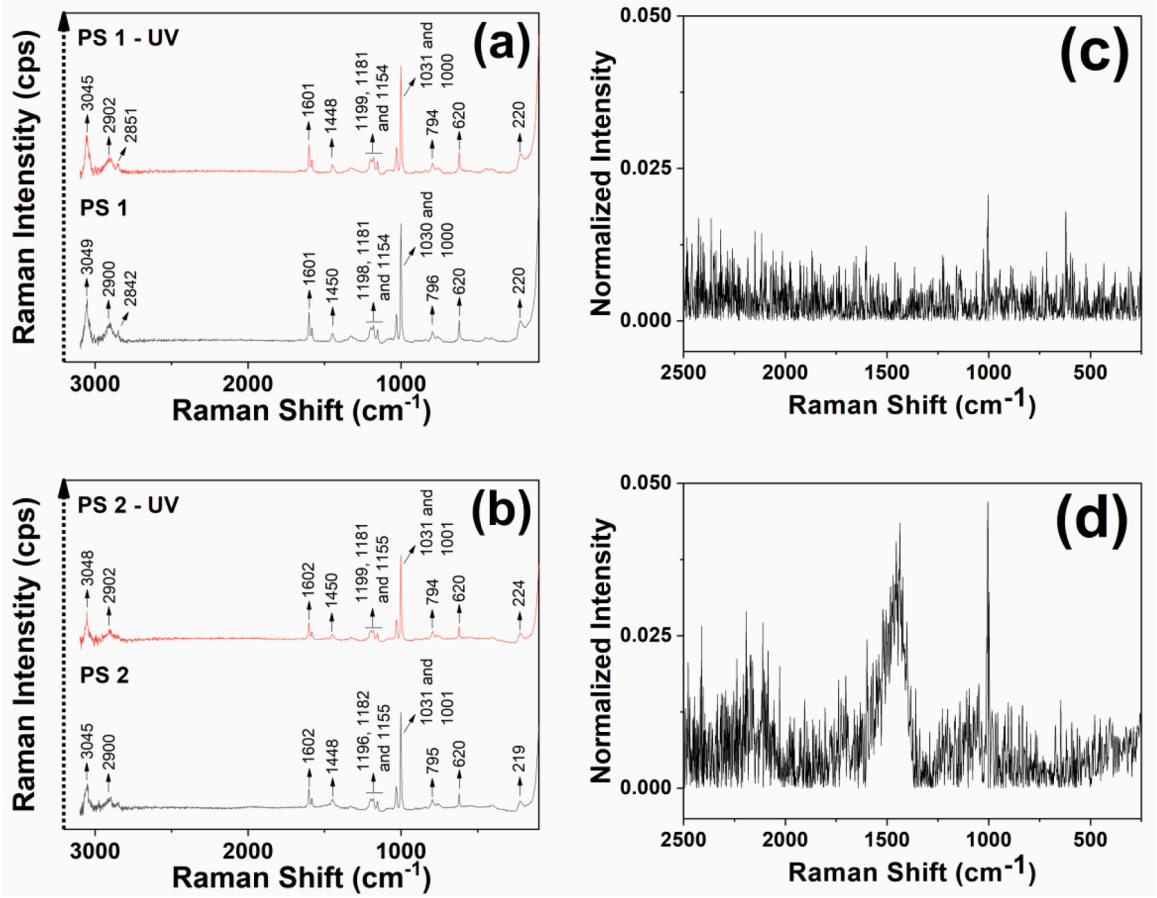

Fig. 3. Raman and normalized Raman spectra of non-irradiated and UVC irradiated polystyrene packaging samples with different thicknesses: (a and c) PS 1 (0.16 mm) and (b and d) PS 2 (0.40 mm). Note that the signal of the UVC-irradiated PS samples has been intentionally shifted to avoid spectral overlapping.

Table 2
Assignment of vibrational modes for observed Raman bands in polystyrene packaging materials.

Wavenumber (cm^{-1})				
Non-irradiated		1 h UVC-irradiated		Assignment of vibrational modes
PS 1	PS 2	PS 1	PS 2	
3049	3045	3045	3048	=C–H stretching vibrations of the aromatic ring
2900	2900	2902	2902	C–H stretching vibrations of the aliphatic group
2842	–	2851	–	CH_3 stretching vibrations
1601	1602	1601	1602	C=C stretching vibrations of the aromatic ring
1582	1583	1582	1583	C=C stretching vibrations of the aromatic ring
1450	1448	1448	1450	Stretching of the aromatic ring and CH_2 scissoring vibrations
1336	–	–	–	CH_2 bending vibrations
1325	1329	1326	1329	CH_2 bending vibrations
1302	–	1302	–	CH_3 bending vibrations
1198	1196	1199	1199	C–C stretches and aromatic C–H in-plane bending vibrations
1181	1182	1181	1181	C–C stretches and aromatic C–H in-plane bending vibrations
1154	1155	1154	1155	C–C stretches and aromatic C–H in-plane bending vibrations
1095	–	1090	–	H–C–H bending and aromatic ring vibrations
1061	–	1063	1070	H–C–H bending and aromatic ring vibrations
1030	1031	1031	1031	C–H in-plane deformation
1000	1001	1000	1001	C=C–H deformation and ring breathing mode
905	–	903	903	C–H out-of-plane vibrations
838	–	–	828	C=C–H deformation
796	795	794	794	C–H out-of-plane deformation and *gauche-gauche* conformation of the aliphatic chain
753	753	757	753	Aromatic group vibrations and C–H out-of-plane vibrations
620	620	620	620	Ring out-of-plane deformation
442	–	445	–	Chain bending or twisting vibrations
401	404	399	403	Chain wagging or twisting vibrations
220	219	220	224	C–C stretching ring and CCC bending ring vibrations

deformation, confirming the presence of a mono-substituted benzene ring mode [23,37,38]; and (ix) 220 cm^{-1}, associated with C–C stretching and CCC bending vibrations of the aromatic ring [23].

The results illustrated in Fig. 3 (a and b) suggest an inverse correlation between the intensity of the Raman signal and the thickness of the PS samples. Specifically, the thinner the sample (PS 1, 0.16 mm thickness), the higher the Raman intensity value (approximately 220 cps at 1000 cm^{-1} compared to PS 2 sample with ~ 150 cps). The phenomenon of Raman shielding typically depends on sample thickness, resulting in a reduction in the measured Raman signal intensity due to light absorption and scattering. These absorption and scattering effects are influenced by the composition, structure and thickness of the sample [40]. In general, the observed Raman bands in non-irradiated PS samples exhibit similarity regardless of their thickness and are consistent with the typical spectrum of the PS molecule [23,37–39].

Nevertheless, it is important to note that the intensity and position of these Raman bands could vary depending on different factors, including the manufacturing process of the polymers, molecular weight and/or degree of crystallinity, among others [41]. For instance, PS with a higher degree of crystallinity may exhibit more pronounced Raman bands because of the increased concentration of PS molecules and a higher level of organization in the polymer chain arrangement [42]. According to the literature [42], PS can exist with two distinct structures: (i) *isotactic* PS, where all pendant methyl groups (-CH_3) on the styrene monomer units are positioned on the same side of the polymer chain, resulting in a highly ordered and *crystalline* structure, and (ii) *atactic* PS, where the pendant methyl groups (-CH_3) are randomly distributed along the polymer chain, leading to a disordered and *amorphous* structure. Therefore, Raman bands around 838 cm^{-1} and 1198 cm^{-1} are dependent on the degree of crystallinity in the sample, and the intensity of these bands could serve as a valuable indicator of PS crystallinity [42]. Consequently, the band centred at 838 cm^{-1}, associated with the C=C–H deformation [23], is more intense in the *isotactic* form compared to the *atactic* form. Additionally, the band around 1198 cm^{-1}, linked to C–C stretches [37] and aromatic C–H in-plane bending vibrations [23], only appears in the spectra of the partially *crystalline* PS samples. Therefore, it can be presumed that both PS samples used in this study may exhibit partial crystallinity, as evidenced by the Raman band peaking at 1198 cm^{-1}. Furthermore, PS 1 material may suggest the *isotactic* form due to its Raman band at 838 cm^{-1}, confirming its highly ordered structure.

In addition, the Raman spectrum of PS materials could exhibit variations subsequent to environmental factors, including temperature fluctuations, chemical treatments (i.e., additives, pigments, antioxidants, among others), and/or exposure to UV radiation. As illustrated in Fig. 3 (a and b), the Raman spectra of UVC-irradiated PS samples present analogous behavior to that previously described for the non-irradiated samples. This observation highlights the robustness of these spectral Raman bands when exposed to UVC radiation treatment and confirms their resistance against further degradation, consistent with the findings from the FTIR characterization.

Thus, (i) the normalized Raman spectrum for PS 1 sample (Fig. 3c) remains practically unaffected, indicating the absence of polymer chain degradation due to exposure to UVC radiation. On the other hand, (ii) upon analyzing the normalized Raman spectrum for PS 2 sample following UVC irradiation in Fig. 3b, slight alterations in the characteristic bands become apparent, suggesting minor alterations in its molecular structure. A weak decrease in Raman signal intensity at 1450 cm^{-1} may suggest a reduction in the stretching vibrations of the aromatic ring and CH_2 scissoring, while a minimum increase around 1000 cm^{-1} could be associated with a slight enhancement of the C=C–H deformation and ring breathing mode.

In summary, these findings indicate that neither of the PS samples exhibit any degradation following UVC irradiation treatment, as observed in the conducted measurements. As previously explained in the FTIR analysis, the observed minimal differences appear to be intrinsic to the characteristics of the PS materials, including their highly ordered structure, molecular weight distribution, additives, among other factors, and may also be influenced by their respective histories, such as prior environmental exposure, manufacturing processes and storage conditions, rather than being attributable to UVC irradiation.

According to the literature [13–17], UVC radiation could cause a *photo-oxidative* degradation, resulting in the breaking of polymer chains (i.e., C–C and C–H bonds), the generation of free radicals (i.e., tertiary alkyl, peroxyl, tertiary alkoxy and keto radicals), and a reduction of the molecular weight of polymers. Therefore, research plays a vital role to study these reactions, the diffusion of free radicals and the physicochemical properties of UVC-irradiated plastics samples.

3.2. UVC-TL emissions of commercial dosimeters (TLD-100, TLD-200, TLD-400 and GR-200)

The study of the shielding of PS materials against UVC radiation is crucial for the precise assessment of potential radiation exposure in the pharmaceutical and medical packaging sectors. To achieve this objective, commercial UVC detectors [26], including TLD-100 (LiF: Ti, Mg), TLD-200 (CaF_2: Dy), TLD-400 (CaF_2: Mn) and GR-200 (LiF: Mg, Cu, P), were used to evaluate the UVC radiation output regarding the thickness of the PS samples. This method allows for a qualitative discrimination between UVC irradiated and non-irradiated PS packaging samples, ensuring its safety and quality in healthcare applications. Furthermore, as previously described, characterization through FTIR and Raman spectroscopy revealed no observable degradation following UVC exposure, thereby confirming the durability of the PS materials under the defined experimental conditions.

These commercial TLDs materials were employed as UVC detectors for the PS samples. Their corresponding UVC-induced TL emissions are illustrated in Fig. 4. Each of these emissions provides valuable insight

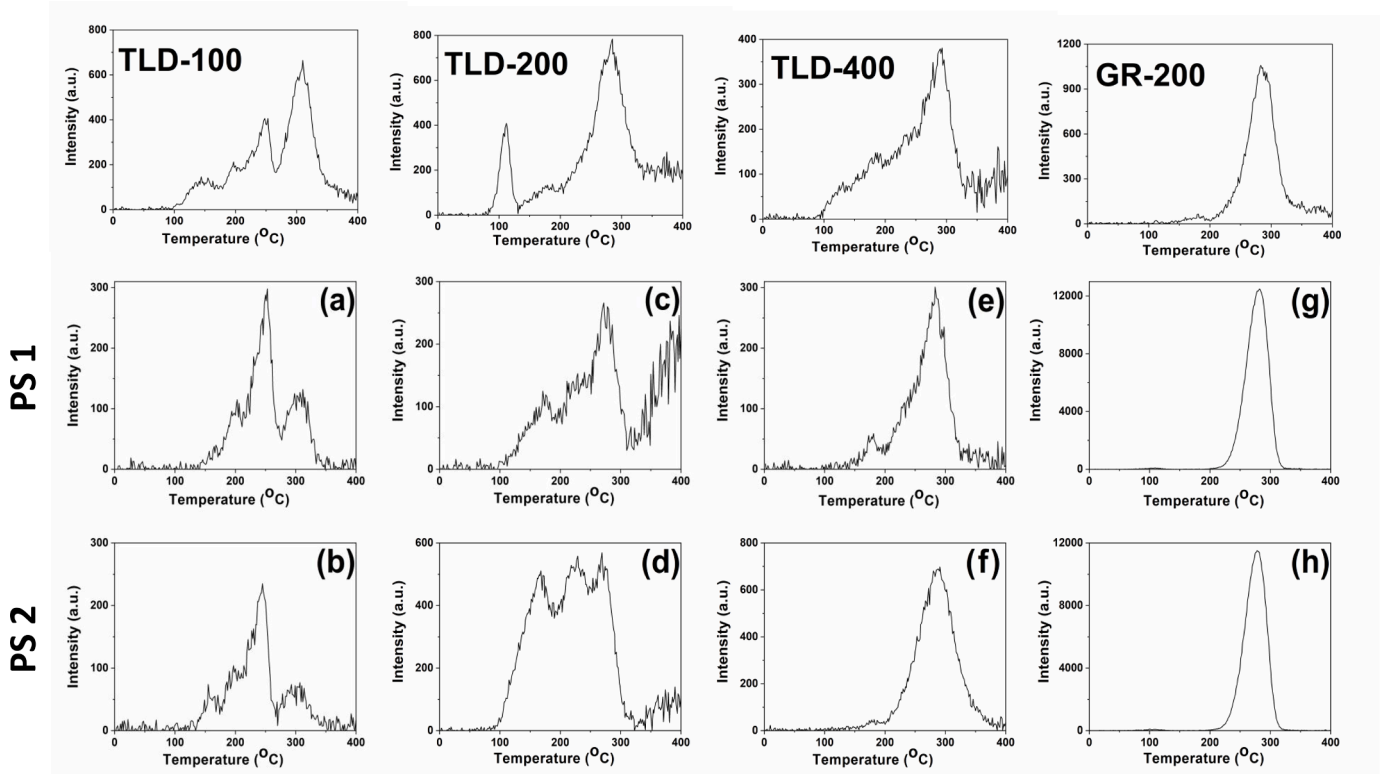

Fig. 4. UVC-induced TL spectra of polystyrene packaging samples with different thicknesses (PS 1 and PS 2, corresponding to the 2nd and 3rd line plots, respectively) and commercial dosimeters (TLD-100, TLD-200, TLD-400 and GR-200, corresponding to the 1st, 2nd, 3rd and 4th columns, respectively). Please note that the 1st line plot represents the UVC-induced TL spectra of the dosimeters without PS packaging samples, as previously studied by Boronat et al. [26].

into the fundamental characteristics associated with the interaction between UVC exposure and the different dosimeters, influenced by the thickness of the PS material.

3.2.1. Effect of UVC radiation on the TL response of TLD-100 (LiF: Ti, Mg)

As illustrated in Fig. 4 (a and b), UVC-induced TL emissions from the TLD-100 dosimeter under PS samples, can be classified into two distinct groups of components: (i) Within the lower temperature range up to ~ 270 °C, the TL glow emission reveals three discernible maxima at ~ 160 °C, ~ 200 °C and ~ 250 °C. These peaks may be entirely associated with the ionizing component of the UVC radiation and could result from the formation of Ti^{4+}– OH^{-} defect complexes in coordination with Mg^{2+} vacancies (also known as Mg-dipoles), as well as with Ti^{4+}– OH^{-}/Mg^{2+}-trimer defect complexes and/or Mg^{2+}dipoles [43]. An ionic radius of 1.37 Å has been determined to be linked to the significant presence OH^{-} ions in the LiF crystal lattice of the TLD-100 material, and several investigations have demonstrated the replacement of F^{-} ions with an ionic radius of 1.33 Å. These hydroxyl groups have a favourable reaction towards the metals found in the TLD-100 material, such as Mg^{2+} and Ti^{4+} ions. As a result, an increase in the concentration of OH^{-} ions within the matrix could increase TL sensitivity [44]. Furthermore, (ii) the TL emission appearing at higher temperatures above ~ 270 °C, predominantly correlates with the non-ionizing component of the UVC radiation. In this case, a single TL emission peak is detected at ~ 310 °C, serving as an indicator of the interaction between the non-ionizing component of UVC radiation and the TLD-100 dosimeter.

Considering the relative intensity values of these two groups of components, PS 1 (Fig. 4a) and PS 2 (Fig. 4b) samples display varying peak intensity ratios, namely 1:3:9:4 and 1:2:4:1, respectively. Specifically, PS 1 sample (Fig. 4a) exhibits its three distinct maxima, related to the ionizing component of the UVC radiation, shifted to higher temperature values, where the most prominent peak is centred at ~ 250 °C. This could suggest that the thinner sample (PS 1, 0.16 mm thickness) may selectively absorb the non-ionizing component of UVC radiation while allowing the ionizing component to pass through. As a result, differences in PS thickness (0.16 and 0.40 mm) used in this study could lead to significant variations in UVC-induced TL glow emissions considering the ionizing component up to ~ 270 °C. Additionally, PS 1 sample (Fig. 4a) display higher sensitivity to UVC radiation due to the signal peaked at ~ 310 °C, which could be linked to the permeability of this thinner sample to the non-ionizing component of UVC radiation.

Consequently, the TLD-100 dosimeter could be a potential UVC radiation detector, primarily owing to the notable signal observed at ~ 310 °C, which is associated with the non-ionizing component of UVC radiation. This emission is particularly pronounced in the thinner PS 1 sample under these measurement conditions.

3.2.2. Effect of UVC radiation on the TL response of TLD-200 (CaF_2: Dy)

As appreciated in Fig. 4 (c and d), the UVC-induced TL emissions from the TLD-200 dosimeter placed under PS samples, indicate the presence of three different groups of components: (i) And (ii) refer to TL glow emissions appearing in the temperature range from ~ 150 °C to ~ 250 °C, with maxima centred at ~ 170 °C and ~ 230 °C. These emissions may be related to the non-ionizing component of UVC radiation. On the other hand, (iii) corresponds to TL emission at higher temperatures from ~ 270 °C and extending up to ~ 350 °C, mainly associated with the ionizing component of UVC radiation. These maxima can be attributed to impurities and structural defects caused by Dy^{3+} ions, which have atomic radii of 1.59 Å and are located within the Ca^{2+} sites (1.74 Å) in the CaF_2 crystal lattice [26].

Taking into account the relative intensity values of these three component groups, the ratios of PS 1 (Fig. 4c) and PS 2 (Fig. 4d) samples are 2:3:5 and 1:1:1, respectively. It is worth noting that the sample thicknesses used in this study (0.16 and 0.40 mm) result in significant fluctuations in the temperature range from ~ 150 °C to ~ 250 °C, which are associated with the non-ionizing component of UVC radiation.

Furthermore, there are differences in the ionizing component of the UVC-induced TL glow emission (peaked at ~ 270 °C). This phenomenon may be related to the ability of the PS samples to allow the transmission of the non-ionizing component of the UVC radiation. Significantly, the increase in both TL signals is more pronounced for the thinner PS sample (PS 1, 0.16 mm thickness).

Thus, consistently displaying response levels within a temperature range from ~ 150 °C to ~ 250 °C (linked to the non-ionizing component of the UVC radiation), the TLD-200 dosimeter proves to be effective in detecting UVC radiation. This observation is particularly evident in both analyzed PS samples, with a more significant effect noted in the thinner PS 1 sample.

3.2.3. Effect of UVC radiation on the TL response of TLD-400 (CaF_2: Mn)

As depicted in Fig. 4 (e and f), UVC-induced TL emissions from the TLD-400 dosimeter under PS samples, can be divided into two groups of components: (i) Several TL glow emissions were observed up to ~ 200 °C, with the maximum peaked at ~ 180 °C. These emissions could be associated with the non-ionizing component of the UVC radiation, as well as structural defects and Mn^{2+} impurities found in Ca^{2+} sites within in the CaF_2 crystal lattice, which have atomic radii of 1.17 Å and 1.74 Å, respectively [45]. And (ii), a broad peak centred at ~ 280 °C, primarily attributed to the ionizing component of UVC radiation.

In this context, the TL signal generated by TLD-400 dosimeter under PS 1 (Fig. 4e) and PS 2 (Fig. 4f) samples displays relative intensity value ratios of 1:6 and 1:18, respectively, for the groups of components centred at ~ 180 °C and ~ 280 °C. The signal has an intensity value of ~ 50 a.u. at ~ 180 °C, suggesting that both PS materials exhibit a similar response to UVC radiation up to ~ 200 °C. This indicates that the thickness of the samples does not significantly affect their UVC response, and both samples have comparable capabilities of transmitting UVC light. On the other hand, PS 2 sample (Fig. 4f) reveals a broad signal peaked at ~ 280 °C, with an intensity value of ~ 700 a.u., which can be associated with the ionizing component of the UVC radiation.

Therefore, the observed dispersion in both TL emissions, wherein a satisfactory correlation between intensity and curve shape with the thickness of the PS samples cannot be established, suggests that the TLD-400 dosimeter might not be a suitable material for UVC detection.

3.2.4. Effect of UVC radiation on the TL response of GR-200 (LiF: Mg, Cu, P)

Fig. 4 (g and h) presents UVC-induced TL emissions of PS samples on a GR-200 dosimeter, where the main signal is peaked at ~ 280 °C and could be due to the ionizing component of the UVC radiation. This emission may be linked to the recombination of crystalline defects, including V_k-e centres (vacancies and electron traps) and H-F defects (color centers in the LiF crystal lattice) [46]. This sensitivity is more evident at higher temperatures (at ~ 280 °C), where no TL signal is present at lower temperatures (at ~ 180 °C). For such reason, GR-200 could detect ionizing radiation, but it is unable to differentiate between ionizing radiation and UVC [26].

Upon examining Fig. 4g and h, PS 1 (0.16 mm) and PS 2 (0.40 mm) samples suggest a similarity as they both show an intensity of around 12,000 a.u. and 11,000 a.u., respectively, in the peak centred at about ~ 280 °C (linked to the ionizing component of the UVC radiation).

4. Conclusions

This study contributes to our comprehension of the interaction between UVC radiation and PS materials, particularly in the realm of post-packaging irradiation processes within healthcare sectors. These findings reveal that UVC radiation has the ability to penetrate PS samples, regardless of their thickness. Nevertheless, the efficiency of this penetration could be affected by the thickness of the PS material. This observation highlights the critical importance for pharmaceutical and medical packaging companies to conduct comprehensive assessments of both the chemical composition and thickness of their materials in order to optimize post-packaging UVC treatment.

These preliminary results suggest that none of the PS packaging samples exhibited significant degradation following UVC irradiation treatment, as evidenced by FTIR and Raman spectroscopy characterization. The observed minimal differences may be attributed to inherent properties of the PS material, such as its crystalline structure, molecular weight distribution, additives, and/or could be linked to their respective histories, including prior environmental exposure, manufacturing processes and storage conditions, rather than the influence of UVC radiation. Therefore, the PS materials demonstrate resilience under these experimental conditions after UVC irradiation treatment. Furthermore, a comprehensive analysis of TL emissions can provide a detailed understanding of the capabilities and limitations of various dosimeter materials used for UVC radiation detection. Specifically, (i) The TLD-100 dosimeter demonstrates potential as a UVC radiation detector, primarily due to the significant signal observed at approximately 310 °C, associated with the non-ionizing component of UVC radiation; (ii) And the TLD-200 dosimeter consistently exhibits response levels within the temperature range of approximately 150 °C to 250 °C, linked to the non-ionizing component of UVC radiation, confirming its effectiveness in UVC radiation detection; (iii) In contrast, the TLD-400 dosimeter may not be a suitable UVC detector, as evidenced by the dispersed TL emissions and the inability to correlate intensity and curve shape with the thickness of the PS samples; (iv) And the GR-200 dosimeter seems unsuitable for UVC detection, as it does not possess the ability to discriminate between ionizing and UVC radiation. These observations were particularly apparent in the analysis of both PS samples, with a more pronounced effect noted in the thinner PS 1 sample (0.16 mm), underscoring the significance of sample thickness in accurate detection and result interpretation.

This methodology consistently demonstrates the capability to detect radiation in healthcare materials one-hour after exposure, thereby enhancing detection reliability even during extended UVC exposures. Consequently, these results could contribute to our scientific understanding, providing practical insights for industries using UVC-PS irradiated materials, particularly in the pharmaceutical and medical applications.

Funding

This research did not receive any specific grant from funding agencies in the public, commercial, or not-for-profit sectors.

CRediT authorship contribution statement

C. Boronat: Investigation, Writing – original draft, Writing – review & editing. **V. Correcher:** Investigation, Writing – review & editing, Supervision. **J. García-Guinea:** Investigation, Writing – review & editing, Supervision. **J.C. Bravo-Yagüe:** Investigation, Writing – review & editing, Supervision.

Declaration of competing interest

The authors declare that they have no known competing financial interests or personal relationships that could have appeared to influence the work reported in this paper.

Data availability

Data will be made available on request.

Acknowledgments

Cecilia Boronat thanks for the predoctoral researcher contract with UNED-SANTANDER associated under the UNESCO Chair, for the support extended under the program "UNESCO Chair on Science and Innovation for Sustainable Development: Global Food Production and Safety".

References

[1] D. Irving, D.A. Lamprou, M. Maclean, S.J. MacGregor, J.G. Anderson, M.H. Grant, A comparison study of the degradative effects and safety implications of UVC and 405 nm germicidal light sources for endoscope storage, Polym. Degrad. Stab. 133 (2016) 249–254, https://doi.org/10.1016/j.polymdegradstab.2016.09.006.

[2] V.R. Sastri, Plastics in Medical Devices: Properties, Requirements, and Applications, Plastics Design Library (PDL), 2022, https://doi.org/10.1016/B978-0-323-85126-8.00002-3. Third Edition.

[3] G. Tamburini, S. Bertagnoli, G. Tarricone, S. Piva, A. Sassella, R. Lorenzi, A. Paleari, Early stages of X-ray induced molecular unit modifications in poly(lactic acid), Polym. Degrad. Stab. 216 (2023) 110485, https://doi.org/10.1016/j.polymdegradstab.2023.110485.

[4] N. Girard-Perier, S. Dorey, F. Gaston, F. Girard, S.R.A. Marque, N. Dupuy, One-year ageing FTIR monitoring of PE/EVOH/PE film after gamma or electron beam irradiation, Polym. Degrad. Stab. 195 (2022) 109790, https://doi.org/10.1016/j.polymdegradstab.2021.109790.

[5] E.I. Epelle, A. Macfarlane, M. Cusack, A. Burns, W.G. Mackay, M.E. Rateb, M. Yaseen, Application of ultraviolet-C radiation and gaseous ozone for microbial inactivation on different materials, ACS Omega 7 (47) (2022) 43006–43021, https://doi.org/10.1021/acsomega.2c05264.

[6] M.C. Celina, E. Martinez, M.A. Omana, A. Sanchez, D. Wiemann, M. Tezak, T. R. Dargaville, Extended use of face masks during the COVID-19 pandemic - Thermal conditioning and spray-on surface disinfection, Polym. Degrad. Stab. 179 (2020) 109251, https://doi.org/10.1016/j.polymdegradstab.2020.109251.

[7] B. Bharti, H. Li, Z. Ren, R. Zhu, Z. Zhu, Recent advances in sterilization and disinfection technology: a review, Chemosphere 308 (3) (2022) 136404, https://doi.org/10.1016/j.chemosphere.2022.136404.

[8] X. Sun, J. Zhuang, X. Ma, Y. Tang, M.M. Ali, Z. Lu, X. Zheng, Z. Du, Structure elucidation and risk assessment of degradation products in gamma irradiated rubber closures, Polym. Degrad. Stab. 204 (2022) 110126, https://doi.org/10.1016/j.polymdegradstab.2022.110126.

[9] M. Silindir, A.Y. Özer, The effect of radiation on a variety of pharmaceuticals and materials containing polymers, PDA J. Pharm. Sci. Technol. 66 (2) (2012) 184–199, https://doi.org/10.5731/pdajpst.2012.00774.

[10] V.R. Sastri, Commodity Thermoplastics: Polyvinyl Chloride, Polyolefins, Cycloolefins and Polystyrene, Plastics Design Library (PDL), 2022, pp. 113–166, https://doi.org/10.1016/B978-0-323-85126-8.00002-3. Third Edition.

[11] M. Demirors, Styrene polymers and copolymers, in: C.D. Craver, C.E. Carraher (Eds.), Applied Polymer Science, 2000, pp. 93–106, 21st Century, https://doi.org/10.1016/b978-008043417-9/50009-x.

[12] D.J. Thomas, 3D printing techniques in medicine and surgery, in: D.J. Thomas, D. Singh (Eds.), 3D Printing in Medicine and Surgery: Applications in Healthcare, 2021, pp. 15–45. https://doi.org/10.1016/B978-0-08-102542-0.00003-8.

[13] A.L. Andrady, A.M. Heikkilä, K.K. Pandey, L.S. Bruckman, C.C. White, M. Zhu, L. Zhu, Effects of UV radiation on natural and synthetic materials, Photochem. Photobiol. Sci. 22 (2023) 1177–1202, https://doi.org/10.1007/s43630-023-00377-6.

[14] N. Nagai, T. Matsunobe, T. Imai, Infrared analysis of depth profiles in UV-photochemical degradation of polymers, Polym. Degrad. Stab. 88 (2) (2005) 224–233, https://doi.org/10.1016/j.polymdegradstab.2004.11.001.

[15] K.C.C. Tse, F.M.F. Ng, K.N. Yu, Photo-degradation of PADC by UV radiation at various wavelengths, Polym. Degrad. Stab. 91 (10) (2006) 2380–2388, https://doi.org/10.1016/j.polymdegradstab.2006.03.017.

[16] D. Rosu, L. Rosu, C.N. Cascaval, IR-change and yellowing of polyurethane as a result of UV irradiation, Polym. Degrad. Stab. 94 (4) (2009) 591–596, https://doi.org/10.1016/j.polymdegradstab.2009.01.013.

[17] E. Yousif, R. Haddad, Photodegradation and photostabilization of polymers, especially polystyrene: review, SpringerPlus 2 (2013) 398, https://doi.org/10.1186/2193-1801-2-398.

[18] S. Kiatkamjornwong, M. Sonsuk, S. Wittayapichet, P. Prasassarakich, P. C. Vejjanukroh, Degradation of styrene-g-cassava starch filled polystyrene plastics, Polym. Degrad. Stab. 66 (3) (1999) 323–335, https://doi.org/10.1016/S0141-3910(99)00082-8.

[19] A.A. Yaseen, E.T.B. Al-Tikrity, E. Yousif, D.S. Ahmed, B.M. Kariuki, G.A. El-Hiti, Effect of ultraviolet irradiation on polystyrene containing cephalexin schiff bases, Polymers 13 (17) (2021) 2982, https://doi.org/10.3390/polym13172982.

[20] D. Zhang, S.M. Dougal, M.S. Yeganeh, Effects of UV irradiation and plasma treatment on a polystyrene surface studied by IR-visible sum frequency generation spectroscopy, Langmuir 16 (10) (2000) 4528–4532, https://doi.org/10.1021/la991353i.

[21] S. Sikandar Shah, I. Ahmad, M. Ishaq, Degradation study of used polystyrene with UV irradiation, Adv. Mater. 2 (3) (2017) 1–6, https://doi.org/10.15761/ams.1000130.

[22] J.F. Rabek, Polymer photodegradation: mechanisms and experimental methods. Polymer Photodegradation, Springer Science & Business Media, 1995.

[23] G. Socrates, Infrared and Raman Characteristic Group Frequencies. Tables and Charts, John Wiley & Sons, 2001. Third Edition.

[24] V. Correcher, C. Boronat, M.D. Virgos, J. Garcia-Guinea, UV-induced thermoluminescence of natural Ca-rich carbonates, J. Appl. Spectrosc. 86 (2020) 1004–1009, https://doi.org/10.1007/s10812-020-00931-5.

[25] V. Correcher, J. Garcia-Guinea, Application of the EN 1788 European standard for the control of saffron, pepper and blends, Food Control 22 (2) (2011) 173–179, https://doi.org/10.1016/j.foodcont.2010.05.020.

[26] C. Boronat, V. Correcher, J.C. Bravo-Yagüe, I. Sarasola-Martin, J. Garcia-Guinea, J. F. Benavente, Comparing the effect of electron beam, beta and ultraviolet C exposure on the luminescence emission of commercial dosimeters, Spectrochim. Acta A Mol. Biomol. Spectrosc. 295 (2023) 122571, https://doi.org/10.1016/J.SAA.2023.122571.

[27] S.W.S. McKeever, Mechanisms of thermoluminescence production in materials for radiation dosimetry, Radiat. Prot. Dosimetry 17 (1986) 431–435, https://doi.org/10.1093/oxfordjournals.rpd.a079854.

[28] A. Delgado, V. Unamuno, J.L. Muñiz, V. Correcher, J.M. Gómez Ros, A simple UV irradiator for low dose reassessment with LiF TLD-100, Radiat. Prot. Dosimetry 67 (4) (1996) 303–306, https://doi.org/10.1093/oxfordjournals.rpd.a031834.

[29] L. Bøtter-Jensen, G.A.T. Duller, A new system for measuring optically stimulated luminescence from quartz samples, Int. J. Radiat. Appl. Instrum. Part D Appl. Radiat. Isot. 20 (4) (1992) 549–553, https://doi.org/10.1016/1359-0189(92)90003-E.

[30] V. Correcher, A. Delgado, On the use of natural quartz as transfer dosemeter in retrospective dosimetry, Radiat. Meas. 29 (3–4) (1998) 411–414, https://doi.org/10.1016/S1350-4487(98)00040-7.

[31] K.G. de Castro Monsores, A.O. da Silva, S. de Sant' Ana Oliveira, R.P. Weber, P. F. Filho, S.N. Monteiro, Influence of ultraviolet radiation on polystyrene, J. Mater. Res. Technol. 13 (2021) 359–365, https://doi.org/10.1016/j.jmrt.2021.04.035.

[32] B.C. Smith, The infrared spectra of polymers III: hydrocarbon polymers, Spectroscopy 36 (11) (2021) 22–25, https://doi.org/10.56530/spectroscopy.mh7872q7.

[33] J.A. Yabagi, M.I. Kimpa, M.N. Muhammad, S. Bin Rashid, E. Zaidi, M.A. Agam, The effect of gamma irradiation on chemical, morphology and optical properties of polystyrene nanosphere at various exposure time, IOP Conf Ser. Mater. Sci. Eng. 298 (2018) 012004, https://doi.org/10.1088/1757-899X/298/1/012004.

[34] J. Fang, Y. Xuan, Q. Li, Preparation of polystyrene spheres in different particle sizes and assembly of the PS colloidal crystals, Sci. China Technol. Sci. 53 (2010) 3088–3093, https://doi.org/10.1007/s11431-010-4110-5.

[35] A.K. Chaudhary, K. Chaitanya, R.P. Vijayakumar, Synergistic effect of UV and chemical treatment on biological degradation of polystyrene by cephalosporium strain NCIM 1251, Arch. Microbiol. 203 (2021) 2183–2191, https://doi.org/10.1007/s00203-021-02228-3.

[36] M.R. Davidson, S.A. Mitchell, R.H. Bradley, Surface studies of low molecular weight photolysis products from UV-ozone oxidised polystyrene, Surf. Sci. 581 (2–3) (2005) 169–177, https://doi.org/10.1016/j.susc.2005.02.049.

[37] T.E. Bridges, M.P. Houlne, J.M. Harris, Spatially resolved analysis of small particles by confocal Raman microscopy: depth profiling and optical trapping, Anal. Chem. 76 (3) (2004) 576–584, https://doi.org/10.1021/ac034969s.

[38] M. Mazilu, A.C. De Luca, A. Riches, C.S. Herrington, K. Dholakia, Optimal algorithm for fluorescence suppression of modulated Raman spectroscopy, Opt. Express. 18 (11) (2010) 11382–11395, https://doi.org/10.1364/oe.18.011382.

[39] G. Xue, J.L. Keonig, Raman spectroscopic study of the orientation of polystyrene in a stretched film and in an adsorbed film, Spectrosc. Lett. 27 (1994) 995–1004, https://doi.org/10.1080/00387019408006648.

[40] K.D. Dahm, D.J. Dahm, Theoretical models of light scattering and absorption, in: Y. Ozaki, C. Huck, S. Tsuchikawa, S.B. Engelsen (Eds.), Near-Infrared Spectroscopy, 2021, pp. 37–60. https://doi.org/10.1007/978-981-15-8648-4_3.

[41] E. Smith, G. Dent, Modern Raman Spectroscopy: A Practical Approach, John Wiley & Sons, 2004, pp. 37–60, https://doi.org/10.1002/0470011831.

[42] B.H. Stuart, Polymer crystallinity studied using Raman spectroscopy, Vib. Spectrosc. 10 (2) (1996) 79–87, https://doi.org/10.1016/0924-2031(95)00042-9.

[43] J.S. Dryden, B. Shuter, The dependence of the thermoluminescence of LiF: Mg^{2+} crystals on the state of aggregation of the Mg^{2+} ions, J. Phys. D. Appl. Phys. 6 (1) (1973) 123–130, https://doi.org/10.1088/0022-3727/6/1/316.

[44] D. Weiss, Y.S. Horowitz, L. Oster, Delocalized recombination kinetic modeling of the LiF:Mg,Ti (TLD-100) glow peak 5 TL system, Radiat. Meas. 43 (2–6) (2008) 254–258, https://doi.org/10.1016/j.radmeas.2007.10.026.

[45] M. Topaksu, V. Correcher, J. Garcia-Guinea, Luminescence emission of natural fluorite and synthetic CaF_2: Mn (TLD-400), Radiat. Phys. Chem. 119 (2016) 151–156, https://doi.org/10.1016/j.radphyschem.2015.10.002.

[46] B. Yang, L. Wang, P.D. Townsend, H. Gao, Comparison between the low temperature thermoluminescence spectra in annealed LiF:Mg,Cu, LiF:Mg,Cu,P and LiF:Mg,Cu,Si, Nucl. Instrum. Methods. Phys. Res. B. 266 (11) (2008) 2581–2586, https://doi.org/10.1016/j.nimb.2008.03.199.